7 Particle Physics at DESY/HERA (H1)

J. Becker, Ilaria Foresti, M. Hildebrandt (until 9/02), N. Keller, J. Kroseberg, L. Lindfeld, Katharina Müller, P. Robmann, S. Schmitt, F. Sefkow (until 7/02)
U. Straumann, P. Truöl, M. Urban, Nicole Werner, and Stefania Xella Hansen

in collaboration with:
R. Baldinger, S. Baumgartner, N. Berger, W. Erdmann, C. Grab, M. Hilgers, B. List, S. Mangano, D. Meer, A. Schöning and R. Weber, Institut für Teilchenphysik der ETH, Zürich; S. Egli, R. Eichler, K. Gabathuler, and R. Horisberger, Paul–Scherrer–Institut, Villigen, and 34 institutes outside Switzerland

(**H1**–Collaboration)

7.1 Electron proton collisions at up to 320 GeV center of mass energy: overall status of the project

Since September 2000 only a limited amount of data has been collected by the H1-experiment, corresponding to an integrated luminosity of $\mathcal{L}_{\rm int} = 9.8$ pb^{-1}. Between the end of the long shutdown for the upgrade of the detector and the accelerator in July 2001 and March 2003, when the accelerator was shut down again, most of the beam time was dedicated to recommissioning the machine, tuning for luminosity, fighting background problems and identifying background sources, and polarisation studies. Even though it could be proven that a specific luminosity $\mathcal{L}_{\rm spec} = 1.80 \cdot 10^{30}$ cm^{-2}s^{-1}mA^{-2} and a beam polarisation of 50 % can be reached, the severe backgrounds and radiation levels limited the beam currents and number of colliding bunches to two thirds of the design values. Hence the peak luminosity has only reached about half of its design value of $\mathcal{L}_{\rm peak} = 4.8 \cdot 10^{31}$ cm^{2}s^{-1}. Even far below this level the tracking devices could not be operated most of the time. More details are given below (Sec.7.2). The analysis of the data taken in 1999/2000 ($\mathcal{L} = 91$ pb^{-1}), combined in some cases with the pre-1999 data ($\mathcal{L} = 50$ pb^{-1}) continued vigorously leading to 16 publications ([1]-[16]) and 30 papers contributed to the 2002 high-energy physics conferences [17] ([18]-[47]), adressing the following subjects:

- neutral and charged electroweak current cross sections, proton structure functions and parton densities (extensions into the lower and higher Q^2 regimes, use of radiative events) [16; 19; 20];
- search for states and interactions outside the standard model: compositeness [40; 48], squarks [40; 48], ν^* [2], e^* [13], leptoquarks [40; 46; 48], single top [45], instantons [9], odderons [12; 38], charged Higgs [42], anomalous lepton pair [41; 43] and W [14; 44] production, anomalous dimensions [40], magnetic monopoles [47];
- photo- and electroproduction of di- and multijets [3; 4; 5; 11; 15; 22; 24; 25];
- photo- and electroproduction of exclusive final states: π^0 [12; 21], ρ [6; 35; 36], J/Ψ [7; 8; 37], Ψ' [10];
- production of open charm and beauty [1; 26; 27; 49; 50];
- diffractively produced final states: inclusive [29; 30; 31; 32; 39], π^0, η [38], jets [33; 34], ρ [6; 35; 36], J/Ψ [37], Ψ' [10];

- photon structure [23].

We will give below an overview of all analyses dealing with physics beyond the standard model (Sec. 7.4.1), and also report on the progress of the analyses, in which University of Zürich group members are involved, namely beauty and prompt photon production, QED Compton scattering and high Q^2 charged current data (Sec. 7.4.2).

Besides the physics analysis the commissioning of our contributions to the upgrade program of the H1-detector occupied most group members (see Sec. 7.3).

7.2 Status of the HERA accelerator

Since the 2000/2001 shutdown, necessary to prepare the HERA II luminosity upgrade, the operation of HERA has been limited to moderate beam currents because of high backgrounds and difficult beam steering requirements. A severe synchrotron radiation background was observed in November and December 2001, limiting the positron current to less than 1 mA. Additional upstream collimators were installed in February and early March 2002, and aperture limitations for the direct synchrotron radiation were removed on the downstream side. Over the following months a positron orbit has been established, which allowed beam currents of up to 30 mA to be stored with tolerable backgrounds. It then became evident that the proton beam-gas background, enhanced by the dynamic pressure increase when raising the positron current, is limiting the tolerable beam currents to about $I_e \cdot I_p < 600\,\mathrm{mA}^2$. With these constraints the maximum integrated luminosity for a given run reached early September 2002 was 80 nb^{-1}, with a specific luminosity near the post upgrade expectation of $2 \cdot 10^{30}$ $\mathrm{cm}^{-2}\mathrm{s}^{-1}\mathrm{mA}^{-2}$. Extensive measurements with a variety of beam conditions have been performed to understand the background effects from synchrotron radiation and from beam-gas interactions. In addition, detailed simulations, especially of the proton background, have been performed. The results of these studies were presented in two reports [51] to the DESY directorate including an extrapolation to the high HERA II design beam currents, of $I_{e,max} = 55$ mA and $I_{p,max} = 135$ mA, and a quantitative evaluation of possible remedies. The limit for safe operation of the H1 detector given above is determined by the currents drawn in the central outer drift chamber (CJC2), which rise beyond the tolerable limit of 150 to 200 μA, and the rate in the silicon pad detector (radiation monitor), which should not exceed its safe limit of about 50kHz.

The behaviour of the CJC currents was studied in HERA runs with single positron and proton beams and during ep collisions. These currents were found to be primarily due to the effects of synchrotron radiation, positron beam-gas and proton beam-gas interactions. Extrapolation to the anticipated HERA-II beam currents leads to an estimated current of about 1 mA in the CJC2, nearly 90% of which is due to proton initiated background. Similarly, the radiation monitor rate, when extrapolated to the design beam currents, is about 400 kHz whereas a rate of 50 kHz is expected from the positron beam alone.

The backgrounds within the H1 detector decreased significantly in the last quarter of 2002 and the quality and quantity of the data taken by H1 has increased accordingly. Problems remained, however, due to a combination of continuous background levels and background spikes. A further reduction in the currents drawn in the CJC by a factor of about three is necessary if safe operation is to be possible with HERA design currents.

In order to optimize the luminosity at high beam currents while respecting the background set limits on the product $I_e \cdot I_p$ the number of filled bunches was reduced in February of 2003. This is useful

since the luminosity is given by

$$\mathcal{L} = \frac{I_e \cdot I_p}{4\pi q^2 N_B f_{\rm rev} \sigma_x \sigma_y} = \mathcal{L}_{\rm spec} \frac{I_e \cdot I_p}{N_B} \ .$$

The space charge limit at injection and the beam-beam effects limit the proton and electron currents to 0.6 mA/bunch and 0.3 mA/bunch, respectively. With a post-upgrade specific luminosity of $\mathcal{L}_{\rm spec} = 1.8 \cdot 10^{30}{\rm cm}^{-2}{\rm s}^{-1}{\rm mA}^{-2}$ one obtains the luminosity values listed in Table 7.1.

Table 7.1: *Luminosity parameters for HERA operation.*

N_B	$I_p^{\rm max}$ [mA]	$I_e^{\rm max}$ [mA]	$I_p \cdot I_e$ [mA^2]	$\mathcal{L}_{\rm peak}$ [10^{31}cm^{-2}s^{-1}]	
119	67	32	2144	2.7	measured 24. 2. 2003
119	72	37	2664	3.3	expected limits
174	108	56	6048	4.8	post-upgrade design
175	94	44	4136	1.4	typical for 2000 running

Further measurements near the end of 2002 and early 2003 and simulations have shown that the tighter acceptances and new magnet configuration following the luminosity upgrade imply that H1 is about 1.5 times more sensitive to backgrounds now than was the case during HERA I operation. The composition of the residual gas has not changed significantly as a consequence of the upgrade. The pressure in the interaction region is higher than prior to the upgrade and is more strongly dependent on the positron current. During the best running conditions achieved to date, the pressure was a factor of about 2 higher than that in 2000. The sensitivity of the H1 central detectors to the pressure in the HERA beam line has been determined as a function of the distance from the detector. Monte Carlo simulations and measurements are in reasonable agreement and imply that sensitivity extends to about 20 m along the proton beam line. Incidents in which the backgrounds are extremely high have caused damage to detectors close to the beam line, in particular to the backward silicon tracker, which according to the evaluation of the thermo-lumiscence dosimeters has received a dose of up to 32'000 Gy. The forward and central silicon trackers have typically doses 400 times less. Heating of elements of the beam line in and around H1 through higher order mode losses at injection energies has been observed and has led to modifications in the design of some elements of the beam line. Current extrapolations indicate that proton induced backgrounds will dominate at HERA II design currents. Improvements in the vacuum therefore remain the primary means of reducing these.

The following modifications are also foreseen: the installation of an ion getter pump at $z = 1.5$ m; improvement of the instrumentation of the vacuum system by installing a residual gas analyser at $z = 3.6$ m; coating of an absorber with molybdenum at 10.8 m to reduce the effects of backscattered synchrotron radiation; protection of the silicon detector and CJC electronics by installing 1 mm of lead shielding around the beam pipe in the region $-150 < z < -70$ cm; alteration of a collimator at $z = -150$ cm (C5B) to reduce scattering of secondaires and also higher order mode heating in this region.

7.3 Summary of group activities related to the H1-upgrade

To cope with the higher luminosity and the more complex background situation a set of five new cylindrical multiwire proportional chambers (CIP2k) was built in Zürich which provide the information which allows to distinguish between beam-gas induced background events and true ep-interactions within 2.3 μs at the first trigger level. Since the development and implementation of this system

binds most of our personal resources, we give some further deails below citing from our recent publications [52; 53; 54]. The project is led by U. Straumann and coordinated at DESY by S. Schmitt.

The five cylindrical chambers with a cathode pad readout have a 16-fold segmentation in azimuth ϕ and a 120-fold segmentation along the beam axis (z), leading to 9600 readout channels. Groups of 60 cathode pads are read out via striplines by a custom designed readout chip (CIPix). It contains an integrating preamplifier and pulse shaping stage for 64 channels. Signals are discriminated (two thresholds are possible) and synchronized to the 10.4 MHz HERA clock. The on-chamber electronics digitizes and multiplexes the data fourfold and sends them via optical links [55] to the trigger and data acquisition system at a rate of about 10 GBit/s. For one progammable channel it is possible to inspect the analog signal, too. Programming is afforded via a standard I^2C interface.

The trigger task is illustrated in Fig. 7.1. By reconstructing the origin of tracks passing through the CIP2k chambers beam gas events are discriminated against physics events from the interaction region. To decide whether an event is a physics or a background event the trigger adds up the number of tracks originating from the nominal interaction region ($n_{\rm phys}$) and compares this number to the sum of the numbers of tracks originating from outside this region in the forward ($n_{\rm forw}$) and the backward ($n_{\rm bac}$) part of the detector with respect to the flight direction of the proton. Events with $n_{\rm phys} < n_{\rm forw} + n_{\rm bac}$ are identified as background, the others as physics events. The trigger algorithm

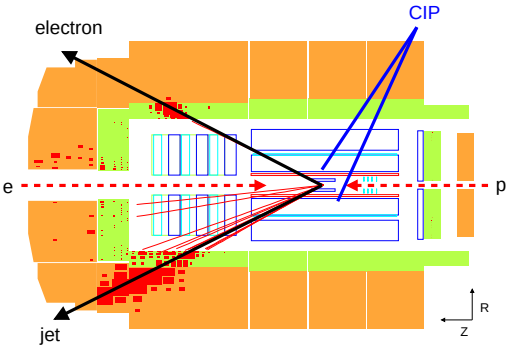

Typical neutral current deep-inelastic scattering event.

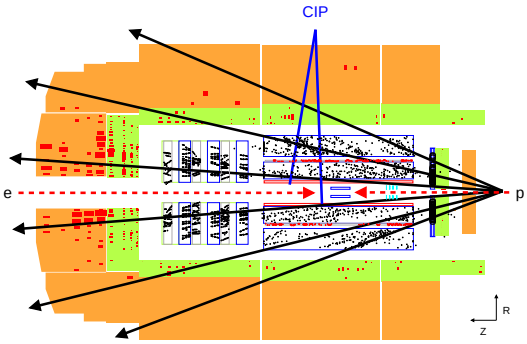

Typical beam-gas event. Most tracks originate outside the nominal interaction region surrounded by the inner tracker.

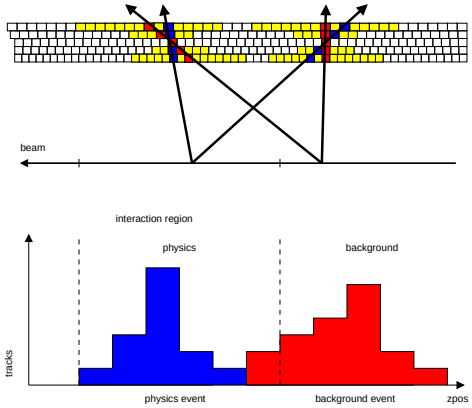

Vertex distribution along the beam axis of tracks crossing the chambers as calculated by the trigger system. From this histogram regions of background and physics tracks can be defined.

Figure 7.1: H1-vertex trigger.

chosen in the CIP2k system is also illustrated in Fig. 7.1. It is separated in three stages - track finding,

- building and - deriving the trigger information from the z-vertex histogram. The tracking algorithm is based on bit pattern comparison of pad data. Field-programmable gate arrays (FPGA) were chosen to accomplish this complex and highly parallelized task. In addition the FPGAs contain pipelines to store the chamber data making it possible to read out the information if a trigger occurs. The trigger, data acquisition and high voltage system are controlled and monitored by the experiment control system (ECS) based on commercial software called PVSSII.

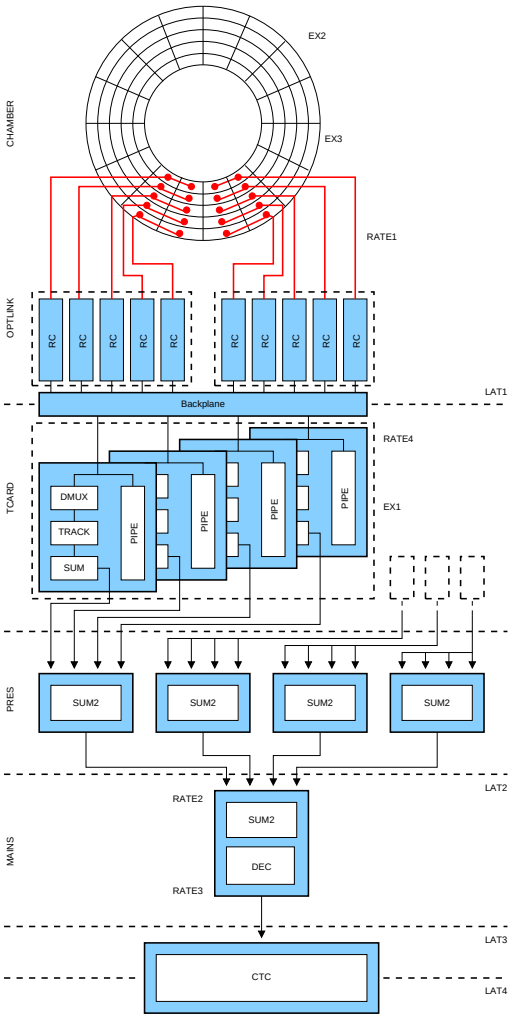

Signal path of the CIP2k trigger system.

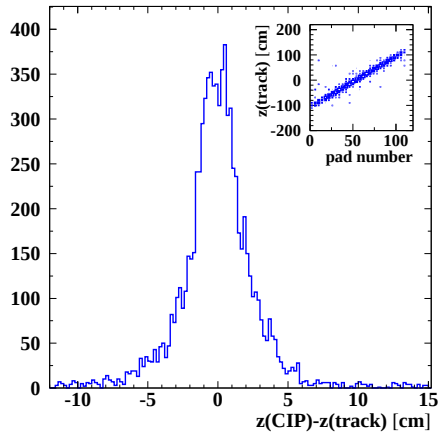

Difference between the CIP hit z-position and the z-coordinate of extrapolated drift chamber tracks. The insert shows the correlation of the CIP2k pad number and extrapolated drift chamber tracks.

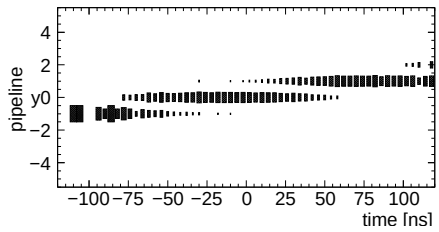

CIP2k trigger pipeline position of the trigger decision with respect to the event timing measured by drift chambers.

Figure 7.2: H1-vertex trigger electronics.

The core of the trigger system (see Fig. 7.2), which is the thesis project of Max Urban, are the custom designed trigger cards (see Fig. 7.3), which contain each two Altera APEX 20K400 FPGAs into which the complete trigger algorithm and the data acquisition pipelines are programmed. These FPGAs were chosen because of the large number of about 500 user I/O pins and the integrated memory pipeline. The trigger card has access to the VME (Versatile Module Europe) bus to read out the data pipeline and to steer the trigger algorithm. The 15 bin wide z-vertex histogram for each ϕ sector is sent via an LVDS link to a custom designed sum card. Each sum card sums up the histogram for four ϕ-sectors. The sum card is equipped with one FPGA (same as on the trigger card). Each sum card builds the z-vertex histogram for one ϕ-quadrant of the chamber. The resulting histograms are sent via an LVDS

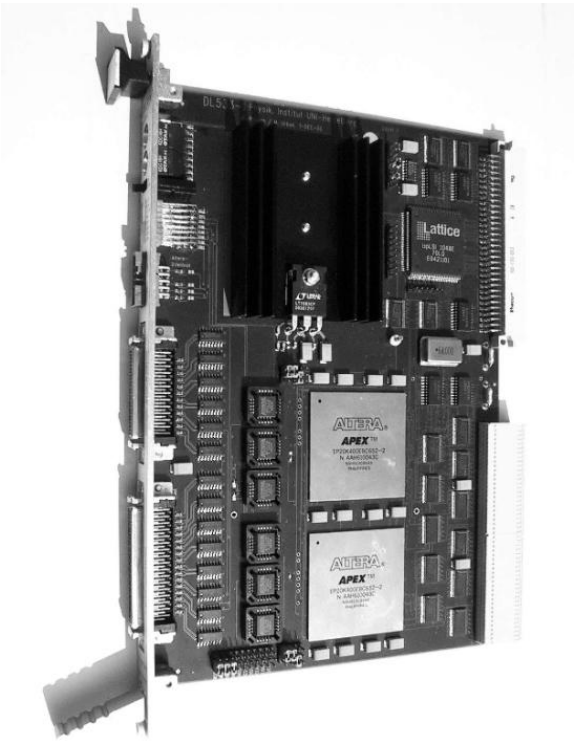

Figure 7.3:
The trigger card. The two FPGAs, the 250 pin input connector on the right side and the micro sub-D connectors on the left side can be seen.

link to the main sum card, which is built as the other sum cards and calculates the global z-vertex histogram for the whole chamber relevant for the 16-bit trigger information for the H1 central trigger system.

The data acquisition system, which is the thesis project of Jan Becker, is based on the VME and the pVIC (PCI Vertical Interconnect) bus system. CPU boards of the type RIO2 8062 with a PowerPC CPU 603 running the real-time operation system LynxOS installed in each trigger crate perform and control the readout of the data from the pipelines in the FPGAs until the arrival of the data at the H1 central data acquisition system. The synchronous part of the data acquisition system with a deadtime constraint of less than 1-2 ms begins with the arrival of a trigger decision starting the readout of the 32 bunch crossing deep pipelines in the FPGAs on the trigger cards. This is done via the VME bus using the single cycle D32/A24 mode with the possibility to switch to an implemented block mode which is not used at the moment. A window of five bunch crossings is read out and grouped into one readout block to study the timing behavior of the trigger system. The readout CPUs arrange the data of the four read out trigger cards in one data package and collect all the packages at one of the CPUs (main CPU) via the pVIC bus. The BMA (block mover accelerator) mode of the pVIC bus is used in this data transfer. The synchronization of the pVIC bus avoiding access conflicts is handled via a custom protocol using the pVIC bus in single cycle mode. With the arrival of the data packages at the main CPU the synchronous part of the readout is finished and the pipelines are ready to be released again. The asynchronous part of the readout starts with the data reduction process in the main CPU. First the chamber data stored as a bit pattern is translated into 16 bit wide pad numbers resulting in an e ective zero suppression if the occupancy of the chamber is less than 10%. Known noisy pads are removed from the data. The data are sent via a VIC link to MEB (Multi Event Buffer) units where they are stored until the H1 central DAQ collects the data from each event via an optical ring.

The system is operational since summer 2001. Early performance tests mainly made use of cosmic muon tracks because of their low rate and clean event signatures. The muon tracks are triggered by the central drift chamber, requiring two track halves opposite in azimuth. The clear correlation between the CIP2k hits and drift chamber tracks and difference between the calculated z-coordinates is

demonstrated in Fig. 7.2. The noise level is negligible, and the width of the distribution is compatible with the expectation from the pad size. This correlation serves as a global test of the chamber, the optical link, and the memory in the FPGAs and DAQ system. Also in Fig. 7.2 the clear correlation between the pipeline position at which the trigger is activated is displayed against the event timing derived from the drift chamber timing. The transition from one pipeline slot to the next slot has a width of about 25 ns which is sufficient to determine the bunch crossings of events from ep collisions. This was demonstrated during 2002/2003 by comparing CIP-timing signals in an offline analysis to event timing without using CIP. Using the CIP timing eliminates the large fraction of non ep events appearing between bunch crossings (see Fig. 7.4).

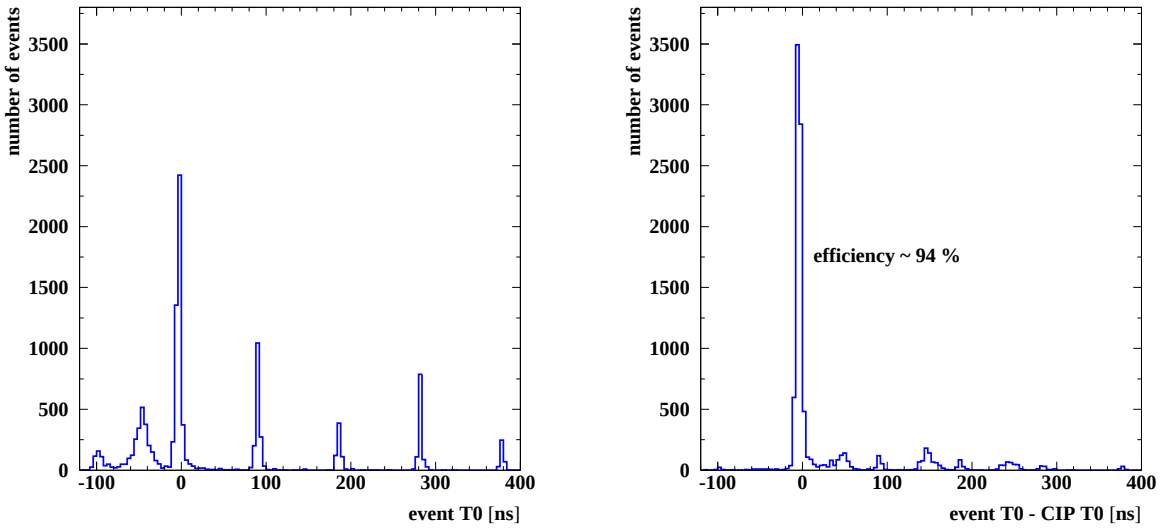

Figure 7.4: *Left: H1 event timing (t_0) at the input of trigger level 4. Bad trigger timing leads to a high rate of non ep events. Right: the same event sample with the CIP2k t_0 applied offline.*

The trigger algorithm has been studied by analysing the simulation of the algorithm on real readout chamber data from cosmic ray events. Due to the cooling problems discussed below only active pads from two out of three layers could be considered. Though the trigger efficiency was found to be high, the separation power for backward, central and forward tracks was yet limited [54], but according to simulations large improvements are expected by running all five layers of the system in the future.

After the initial tests of the chamber performance in 2001 a variety of problems related to insufficient cooling developed. The ambient temperature produced by the central jet chamber electronics is so high, that the CIPix reaches temperatures near 50°C with the normal cooling circuit running at 17°C. At these temperatures instabilities in the addressing of some CIPix chips occurred at first, and later a complete loss of their functionality was observed. A subsequent laboratory test confirmed that at these high temperatures wires bonded to the chips can break, which explains the loss of connection. As a counter measure a separate cooling circuit was installed with an operating temperature of 8°C, which kept the CIPix temperature below 40°C. However, out of the five chamber layers the outermost two were partly lost before the roots of the problem were discovered. The whole frontend electronics has now been rebuilt in such a way, that the bond breaking can no longer occur, and has been replaced during the ongoing shutdown. Additional cooling lines are being added to the chamber electronics, too.

Whenever the central drift chamber was switched on during HERA luminosity runs, the CIP was switched on, too. The design and implmentation of the CIP slow control (i.e. chamber HV and

current as well as temperature monitoring and control, on-line monitoring of the chamber efficiency) is part of the thesis project of N. Werner. The temperature monitoring e.g. is used to automatically switch off the supply voltages if a limit is exceeded. The CIPix chips have proven to be stable and the different programming options quite useful during HERA operation. Having the analog signal available allowed for optimisation of the timing as well as the signal to noise ratio. No sign of radiation damage has been observed. After replacement of the damaged boards on the chamber and on-chamber readout tests the CIP will be reinstalled in the H1 detector early May 2003.

7.4 Results from recent analyses

7.4.1 Search for physics outside the Standard Model

Contact interactions and leptoquarks

Many proposed extensions to the Standard Model (SM) would manifest themselves in the HERA ep data at large momentum transfer. Examples discussed below are composite models, leptoquarks, supersymmetry and extra dimensions. The most recent H1-analysis [40; 48] is based on three data sets comprising a total integrated luminosity $\mathcal{L}_{\rm int}$ 117.2 pb^{-1} (Tab. 7.2), and extends an earlier analysis based on the pre-1998 data [58].

Table 7.2: *Data sets used in the search for exotics analysis.*

Reaction	$\mathcal{L}_{\rm int}$ [pb^{-1}]	$\sqrt{s}$ [GeV]	Run period	Ref.
$e^-p \to e^-X$	16.4 ± 0.3	319	1998 - 1999	[57]
$e^+p \to e^+X$	65.2 ± 1.0	319	1999 - 2000	[16]
$e^+p \to e^+X$	35.6 ± 0.5	301	1994 - 1997	[56]

The new cross section data $d\sigma(e^-p \to e^-X)/dQ^2$ [57] and $d\sigma(e^+p \to e^+X)/dQ^2$ [16] are shown in Fig. 7.5. Over six orders of magnitude the data are well described by a next-to-leading order deep inelastic scattering calculation using the CTEQ5D parton distributions [59]. In order to compare the different models with the data the predicted cross sections are reweighted at each Q^2 by the ratio of the leading order cross section with and without inclusion of the contact interaction (CI) $\hat{\sigma}^{LO}(SM + CI)/\hat{\sigma}^{LO}(SM)$. For any particular model the most general form of the chiral invariant vector-like four-fermion contact interaction Lagrangian

$$\mathcal{L}_V = \sum_q \sum_{a,b=L,R} \eta^q_{ab} (\bar{e}_a \gamma_\mu e_a)(\bar{q}_b \gamma_\mu q_b) \; ,$$

with an appropiate choice of couplings $\eta^q_{ab} = \epsilon_{ab}(g/\Lambda^q_{ab})^2$ can be used. Here a and b indicate the left-handed (L) and right-handed (R) fermion helicities, g is the the overall coupling strength, Λ^q_{ab} is a scale parameter and ϵ_{ab} determines the sign of the interference term.

In general models allowing for compositeness or substructure it is convenient to choose a coupling strength of $g^2 = 4\pi$ and to assume a universal scale Λ for all quarks: $\eta^q_{ab} = \epsilon_{ab}(4\pi)/(\Lambda^2)$. Various chiral structures, pure left, right, vector or axial vector couplings are chosen by setting $e_{ab} = \pm 1$ and putting all other contributions to zero. Lower limits at 95 % CL on the scale parameters $\Lambda^\pm$ range between 1.6 and 5.5 TeV depending on the chiral structure.

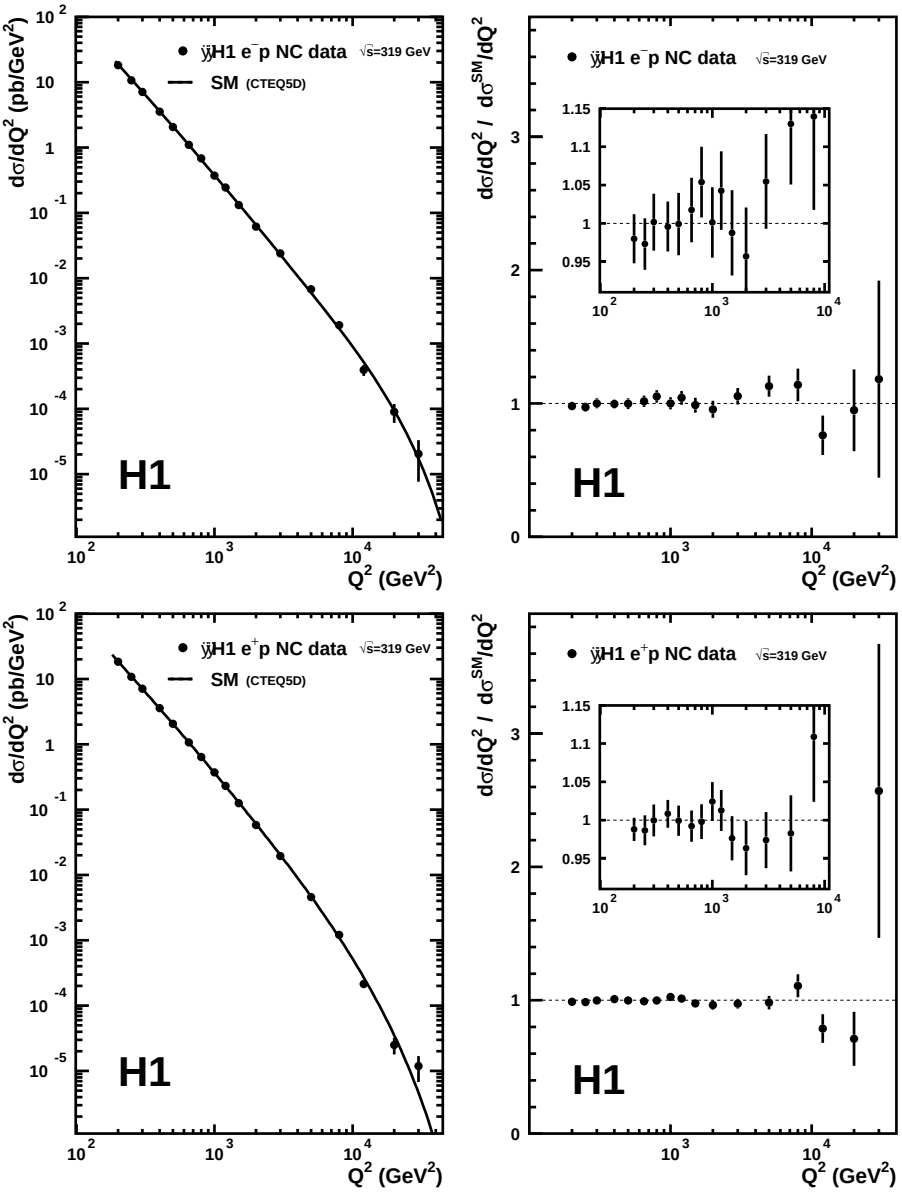

Figure 7.5: Differential cross sections $d\sigma/dQ^2$ at $\sqrt{s} = 319$ GeV for $e^-p \to e^-X$ scattering (top) and $e^+p \to e^+X$ scattering (bottom), compared to SM expectations using the CTEQ5D parton distributions. A preliminary version of these data was shown in the 2000/1 annualreport.

Leptoquarks couple to lepton-quark pairs and appear in extensions of the SM which connect the lepton and the quark sectors. They are colour triplet scalar or vector bosons, carrying lepton (L) and baryon (B) number and a fermion number $F = L + 3B$, with $F = 2$ for e^-q and $F = 0$ for e^+q states. For high enough scales the leptoquark mass M_{LQ} and its coupling are related to the contact interaction coefficients via $\eta^q_{ab} = \epsilon^q_{ab}(\lambda^2)/(M^2_{LQ})$. Lower limits on the ratio M_{LQ}/λ between 0.3 and 1.4 TeV are found.

A more detailed analysis [46] of the full 1994 - 2000 data sample with $Q^2 > 2500$ GeV^2 and $0 < Q^2/M^2 < 0.9$, requiring an identified electron with transverse momentum above 15 GeV/c (neutral current interactions) or a missing transverse momentum above 25 GeV/c (charged current

interactions), set limits on leptoquark production in the s-channel. Leptoquarks decaying to eq or νq in s-channel are produced at a mass $M = \sqrt{s_{ep}x}$, where x is the momentum fraction of the proton carried by the interacting quark. Masses below 300 GeV are accessible this way. In addition exchange of a leptoquark in the u-channel between the incoming lepton and a quark from the proton is possible. The amplitudes for these processes interfere with those from normal deep-inelastic scattering. The analysis updates an earlier one [60] and considers those mass domains, where the resonant s-channel dominates the leptoquark signal cross section. The analysis excludes leptoquarks with electromagnetic coupling strength and masses below 290 GeV, extending exclusion plots from Tevatron experiments into the mass range above 200 GeV.

In the most general formulation of supersymmetry there exist couplings between a lepton-quark pair and a squark, the scalar superpartner of a quark. Such couplings violate R-parity (via lepton number violation $\Delta L \neq 0$), defined as $R_p = (-1)^{3B+L+2S}$ with S being the spin. This interaction allows single squarks to be produced or exchanged in deep inelastic scattering via

$$e^+ d_R \to \tilde{u}_L,\, \tilde{c}_L,\, \tilde{t}_L \;:\; \text{coupling } \lambda'_{1j1}\,; \qquad e^+ \tilde{u}_L \to \bar{\tilde{d}}_R,\, \bar{\tilde{s}}_R,\, \bar{\tilde{b}}_R \;:\; \text{coupling } \lambda'_{11k}\,.$$

The subscripts ijk describe the generation indices of the left-handed leptons, left-handed quarks and right-handed down-type quarks of the superfields, respectively. Squarks with masses satisfying $M_{\tilde{u}}/\lambda'_{1j1} < 0.43$ TeV and $M_{\tilde{d}}/\lambda'_{11k} < 0.71$ TeV can be excluded.

It has been suggested that the gravitational scale M_S in $4+n$ dimensional string theory may be as low as the electroweak scale of order TeV [61]. The relation to the Planck scale $M_P \approx 10^{19}$ GeV and the size R of the n compactified extra dimensions is given by $M_P^2 = R^n M_S^{2+n}$. In some models with large extra dimensions the SM particles reside on a four-dimensional brane, while the spin 2 graviton propagates into the extra spatial dimensions and appears in the four-dimensional world as a tower of massive Kaluza-Klein states with a level spacing $\Delta m = 1/R$. Though the gravitons couple to the SM particles via the energy-momentum tensor with a tiny strength given by the Planck scale, the summation over the enormous number of Kaluza-Klein states up to the ultraviolet cut-off scale, taken as M_S leads to an effective contact-type interaction with coupling $\eta_G = \lambda/M_S^4$. The details of the calculation of the cross section have been given in [58]. The interference between the graviton

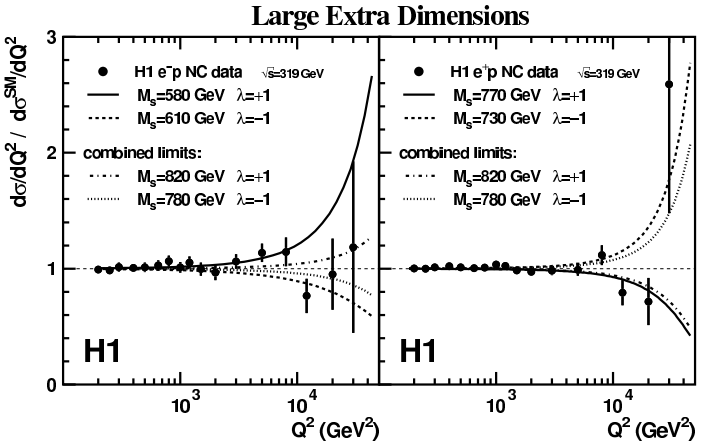

Figure 7.6: *Neutral current cross sections $d\sigma/dQ^2$ at $\sqrt{s}$ =319 GeV normalised to SM expectation. The data are compared to the 95 % CL exclusion limits obtained from each data set and the combined data for gravitational scales M_S assuming positive ($\lambda = +1$) or negative ($\lambda = -1$) coupling.*

and the photon has opposite sign for electron and positron scattering as illustrated in Fig. 7.6. Lower limits on the scale parameter are given in Table 7.3.

A fermion substructure can also be formulated by assigning a finite size to the electroweak charge distributions. It is convenient to introduce electron and quark form factors $f(Q^2)$ which reduce the

Table 7.3: *Lower limits (95 % CL) on the gravitational scale M_S assuming positive ($\lambda = +1$) and negative ($\lambda = -1$) coupling from the e^-p, e^+p and combined $e^-(e^+)p$ data (top part). Upper limits (95 % CL) on the quark radius assuming point-like leptons ($f_e \equiv 1$) or common form factors ($f_e = f_q$) from the e^-p, e^+p and combined $e^-(e^+)p$ data (bottom part).*

	e^-p (319 GeV)	e^+p (319 GeV)	all e^-p & e^+p
Coupling	M_S [TeV]	M_S [TeV]	M_S [TeV]
$\lambda = +1$	0.58	0.77	0.82
$\lambda = -1$	0.61	0.73	0.78
Form factor	$R[10^{-18}\mathrm{m}]$	$R[10^{-18}\mathrm{m}]$	$R[10^{-18}\mathrm{m}]$
$f_e \equiv 1$	1.1	1.1	1.0
$f_e = f_q$	0.8	0.8	0.7

SM cross section at high momentum transfer

$$f(Q^2) = 1 - \frac{\langle r^2 \rangle}{6} Q^2 \ , \quad \frac{d\sigma}{dQ^2} = \frac{d\sigma^{SM}}{dQ^2} f_e(Q^2) f_q(Q^2) \ .$$

Upper limits for $R = \sqrt{\langle r^2 \rangle}$ are given in Table 7.3, too. Analyses performed by other experiments at HERA, LEP and the TEVATRON are providing results similar to ours.

Higgs-, single top-, and W-production

The measurement of rare processes in ep interactions at HERA provides a unique method to search for new physics. Particularly suitable are those final states where high transverse momentum (p_T) leptons are produced. The H1 collaboration analysed quite a few different channels and compared the cross sections to SM model expectations. No statistically significant deviations have been found so far, but some anomalies appear, which need to be substantiated or refuted by HERA II data. In the following a summary of these results is given[3].

Multi-lepton production at high transverse momentum is dominated in the SM by the interactions of quasireal photons radiated by the incident electron and proton leading to a lepton pair ($\gamma\gamma \to \ell^+\ell^-$). For multi-electron final states data corresponding to $\mathcal{L}_{\mathrm{int}} = 115$ pb^{-1}have been analysed [41]. At least two electrons with $20^\circ < \theta_e < 150^\circ$ and $p_T(1) > 10, p_T(2) > 5$ GeV are required in the sample, which comprises 105 $2e$ events and 16 $3e$ events. Good overall agreement is found with the SM predictions, dominated by photon-photon interactions. Six events are observed with a di-electron mass above 100 GeV, where the SM prediction is 0.5. A subsample of 41 events is identified with the $\gamma\gamma$ process by requiring $2e = e^+e^-$ and $\sum E_i - P_{Li} < 45$ GeV (fractional incoming electron energy loss $y < 0.82$). The expected rate within the accepted kinematical region is 48 ± 6. This analysis is the first of its kind at HERA. A similar analysis for muon pair production [43] ($\mathcal{L}_{\mathrm{int}} = 71$ pb^{-1}, $M_{\mu\mu} > 5$ GeV, $p_{T\mu} > 2$ GeV) finds good agreement with the SM model predictions. In the data sample 1243 events were found, while 1253 ± 125 were expected. Figure 7.7 shows the di-muon mass distribution.

The search for the single production of doubly-charged Higgs bosons ($H^{\pm\pm}$) is motivated by the observation discussed above of a few multi-electron events with a large di-electron mass, in a domain

[3]If not explicetely mentioned otherwise the term *electron* describes generically electrons and positrons here

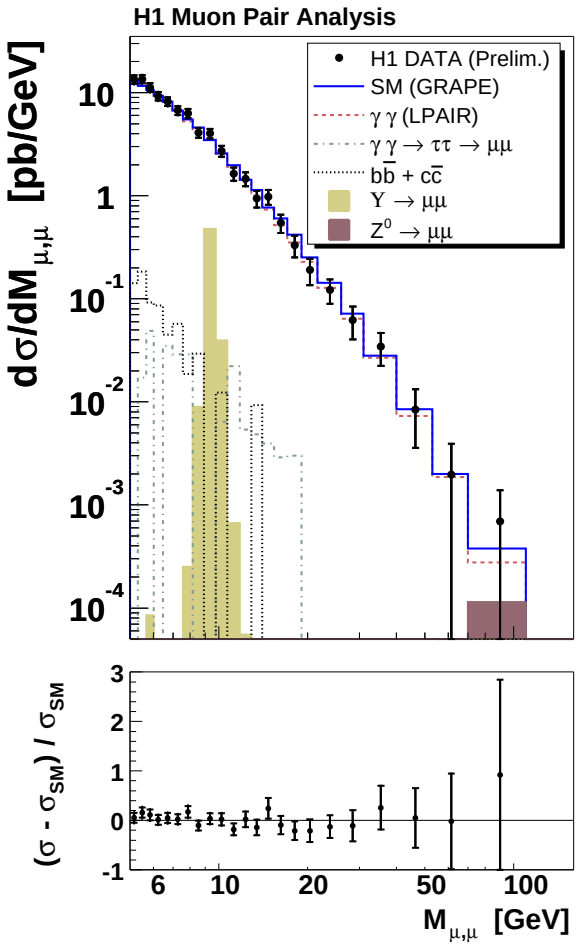

Figure 7.7: *Invariant di-muon mass distribution compared to electroweak SM predictions calculated with the Monte Carlo generator GRAPE [62]. The contributions for the most important processes are indicated separately.*

where the SM expectation is small. It is performed in the framework of models where a Higgs triplet is coupled to leptons of the i^{th} generation via Yukawa couplings h_{ii}. The signal is searched for in the decay modes $H^{\pm\pm} \rightarrow e^{\pm}e^{\pm}, \mu^{\pm}\mu^{\pm}$ using the H1-multi-lepton data sample [42]. Only one of the multi-electron events is found to be compatible with the hypothesis of the decay of a heavy Higgs boson. Assuming that the doubly-charged Higgs only decays to electrons, a lower limit of about 131 GeV can be set on the $H^{\pm\pm}$ mass for a value $h_{ee} = 0.3$ of the coupling, which corresponds to an interaction of electromagnetic strength. This is the first search for doubly-charged Higgs production at HERA.

The search for anomalous top quark production mediated by a flavour changing neutral current via a γut-coupling again the data from an integrated luminosity of $\mathcal{L}_{\rm int} = 115$ pb^{-1} [45]. The top decays into a b-quark jet and a W boson are considered in both the leptonic and the hadronic decay modes of the W. In the leptonic decay modes, five events are found to be compatible with the hypothesis of anomalous top quark production while 1.8 events are expected from the SM. No excess above the SM expectation is found in the hadronic decay channel. An upper limit on the anomalous γut-coupling of $\kappa_{\gamma,u} = 0.22$ is established in the framework of recent NLO calculations [63].

The H1 experiment has reported an excess of events with an isolated lepton, missing transverse momentum and a high E_T hadronic system [14]. We have reported on this in previous annual reports. The kinematics of these events are mostly compatible with a leptonic W decay. While in e^-p scattering ($\mathcal{L}_{\rm int} = 13.6$ pb^{-1}) no events were found consistent with the expectataion for this low luminosity sample, in e^+p ($\mathcal{L}_{\rm int} = 101.6$ pb^{-1}) 18 events were found compared to an expected 10.5 ± 2.5 dominated by W production (8.2 ± 2.5). The excess above the expectation is mainly due to events with transverse momentum of the hadronic system greater than 25 GeV where 10 events are found compared to 2.8 ± 0.7 expected. This prompted a new analysis looking for W production in the jet decay channel. Jets are selected using the inclusive k_T algorithm with a minimum transverse energy of 25 GeV. The phase space has been optimised to maximise the acceptance for W events and to reject other SM processes. No deviation from the SM is found up to highest values of p_T^X, the transverse momentum of the hadronic system. For $P_T^X > 40$ GeV, 25 events are found compared to 2.3 ± 0.7 expected from W-production and 25.9 ± 6.5 from other QCD processes.

7.4.2 Progress of Zürich analysis projects

Prompt photon production

ep collisions at HERA are dominated by electron scattering at small angles with a quasi real photon interacting with the proton (γp collisions). These interactions can also lead to the emission of photons - so called prompt photons - from the hard QCD process, which makes them sensitive both to the partonic structure of the proton and the photon. Events, in which a hard, prompt photon instead of a gluon is emitted depend much less on the fragmentation or hadronisation models since a direct observation of a particle from the hard subprocess is possible. This considerably reduces the systematic error in the determination of the momentum fraction of the partons of the scattering process, and is therefore a better method than the study of dijet-events, which so far has been used, because the full integrated luminosity from the years 96-00 was not available yet.

Prompt photons are identified in the H1 liquid argon calorimeter (LAR) by a compact electromagnetic cluster with transverse energy 5 GeV$< E_T^\gamma <$ 10 GeV in the pseudorapidity region $-1 < \eta^\gamma < 0.9$. No track is allowed to point to the candidate. The main experimental difficulty is the separation from hadronic background. The signal from neutral mesons (π^0 or η^0) at high energies is very similar to the signal of a photon since the decay photons cannot be resolved in the calorimeter. Most of these mesons are associated by a hadronic jet, therefore the photon candidate is required to be isolated. The range of y ($0.2 < y < 0.7$) corresponds to a γp center of mass energy of $142 < W < 266$ GeV.

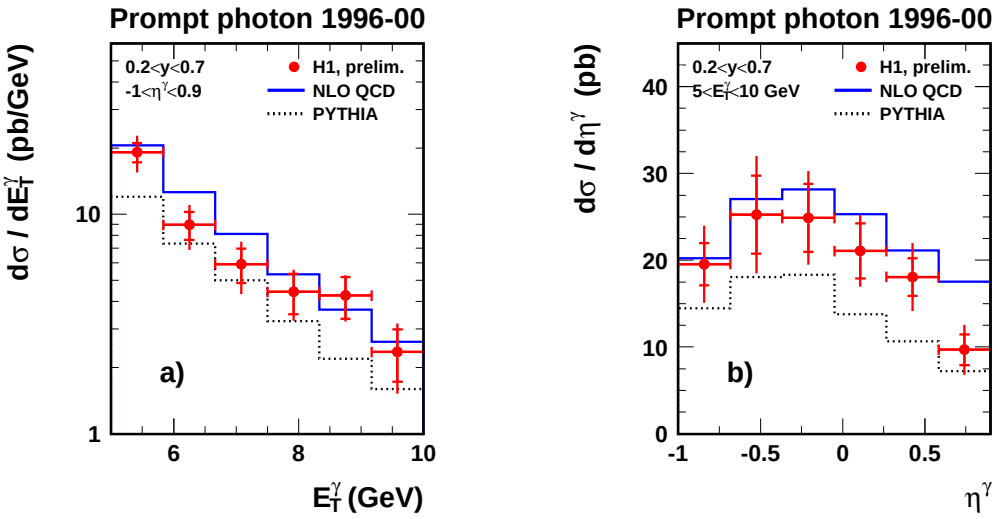

Figure 7.8: *Cross section for prompt photon events as a function of transverse momenta (a) and pseudorapidity η (b) of the photon. The result is compared to LO-Monte Carlo (black) and NLO(blue) calculation.*

First results of this analysis based on $\mathcal{L}_{\rm int} = 102$ pb^{-1} are now avalable [23]. Figure 7.8 shows the prompt photon cross section as a function of transverse energy (a) and pseudorapidity (b). The results are compared to the PYTHIA Monte-Carlo and a NLO-QCD calculation[64]. Both models describe the shape of the data quite well, but not the magnitude.

The measurement will be extended (K. Müller) into the region of high E_T photons as well as into the forward region of the detector to gain more sensitivity on the resolved component of the photon. This will require a detailed knowledge of both the detector response and the detector simulation. Furthermore events with a hadronic jet together with the isolated photon will be selected in order to reconstruct the parton momenta in the photon and the proton.

Beauty production

A strong focus of our physics analysis activities within the H1 collaboration in the past years has been the field of heavy quark production [49]. The interest is twofold: charm production accounts for a large proportion – about 25% – of the total deep inelastic scattering rate at HERA. Understanding the heavy quark production process thus forms a vital ingredient to the proton structure function analysis of inclusive DIS data. Since it is, in the theoretical framework of QCD, a mostly gluon induced reaction, it is particularly suited to enlighten the rôle of gluons in hadronic structure. On the other hand, the heavy quark mass induces a scale in the calculations which renders perturbative methods applicable, such that QCD is relatively predictive for heavy flavour production and allows meaningful tests of the concepts. The fact that the observable hadrons to a large extent inherit the kinematics of the primordially produced quarks provides direct insight into production dynamics at the level of the hard-interacting partons. In contrast to what may be expected on the basis of the large b quark mass, the predictions for beauty production do not well match the experimental data obtained in $\bar{p}p$ collision experiments, or recently from two photon interactions. The HERA data are in similar conflict with theoretical expectations which are based on common methods for these different production modes.

These results received considerable interest; they relate HERA to other environments and communities and demonstrate that there are still open issues in perturbative QCD, to which ep collisions provide particularly viable access. Experimentally, the subject relies strongly on track-based triggering and on precise track and vertex reconstruction, and it thus complements well the contributions to the detector construction made by our institute.

Five PhD thesis projects on heavy quark production have been performed in our group, under supervision of F. Sefkow, who is since last year also acting as convenor of the heavy flavour physics working group in H1. Three theses, on charm production in DIS, in photo-production, and in diffractive interactions, have been completed some time ago and all resulted in journal publications. The electroproduction analysis has recently been updated using a statistically larger data set ($\mathcal{L}_{\rm int} = 48$ pb^{-1} [27], making use of the separation of the D^* decay vertex from the ep-vertex. The thesis of J. Kroseberg on beauty production [50], which pioneered this use of the central silicon tracker information in the H1-analysis, presented the first measurement of b quark production in deep inelastic scattering [26].

In a new approach, explored in the thesis project of I. Foresti, heavy flavoured hadrons are tagged using secondary vertex techniques, which take advantge of the long life-time. The analysis is performed on a sample of μ tagged dijet events. To build up a b-tagging tool, the combined probability for a group of tracks to come from a common origin (the primary vertex of the event) is calculated, and used as a discriminating variable. With the same method used in the μ analysis, the quantities $P_{T,rel}$ (P_T of the track with respect to the jet axis it belongs to) and δ (signed impact parameter) are calculated for the muon. A fit on the distribution of $P_{T,rel}$ against δ gives the decomposition of the data sample (reference spectra from the Monte Carlo distributions of $b\bar{b}$, $c\bar{c}$ and light quark samples). Cutting on the combined probability, it is possible to reject non b events. This analysis has been interupted due to a motherhood leave, but is going to resume soon with the help of S. Xella and will be extended to include the 1999/2000 data, too.

High Q^2 charged current data

As part of the upgrade project the H1 collaboration also changes its software tools to object oriented programming. Within this new analysis frame charged current (CC) data at high Q^2 taken during the last pre-upgrade run 1999/2000 are being analysed by Nicole Werner for her thesis project. The goal of this analysis is a reevaluation of the CC cross section. The analysis has progressed to a point,

where satisfatory initial agreement between the old and the new analysis approach has been reached in all control variables and nearly all bins in Q^2 and x. Fine tuning is in progress.

QED Compton scattering

QED Compton scattering [65] in high energy ep collisions denotes the reaction $ep \to e\gamma X$. In the elastic case ($X = p$) the characteristic event signature is a nearly coplanar electron-photon pair with typically 10 GeV of energy, observed at a finite angle within the detector, with no other activity in the calorimeter, in contrast to Bethe-Heitler bremsstrahlung, where both e and γ escape under small angle, and are possibly detected by the luminosity system. The process was first observed at HERA by H1 [66], and can be used for a measurement of the luminosity (cross check), electromagnetic calibration of the detectors, search for excited electrons e^*, the photon content of the proton and the measurement of F_2 at small Q^2 and large x. For the latter two aspects the inelastic process ($X \neq p$) is used. The analysis, which is the basis of N. Keller thesis, deals with both the elastic and the inelastic channel and the data up to 1997, and is nearly completed.

[1] *Measurement of $D^{*\pm}$-Meson Production and F_2^c in Deep-Inelastic Scattering at HERA*, H1-Coll. C. Adloff *et al.*, DESY 01 – 100, hep-ex/0108039, Phys. Lett. **B528** (2002), 199 - 215

[2] *Search for Excited Neutrinos at HERA*, H1-Coll., C. Adloff *et al.*, DESY 01 – 145, hep-ex/0110037, Phys. Lett. **B525** (2002), 9 - 16.

[3] *Measurement of Dijet Electroproduction at Small Jet Separation*, H1-Coll., C. Adloff *et al.*, DESY 01 – 178, hep-ex/0111006, Eur. Phys. J. **C24** (2002), 33 - 41.

[4] *Measurement of Dijet Cross Sections in Photoproduction at HERA*, H1-Coll., C. Adloff *et al.*, DESY 01 – 225, hep-ex/0201006, Eur. Phys. J. **C25** (2002), 13 - 23.

[5] *Energy Flow and Rapidity Gaps between Jets in Photoproduction at HERA*, H1-Coll., C. Adloff *et al.*, DESY 02 – 023, hep-ex/0203011, Eur. Phys. J. **C24** (2002), 517 - 527.

[6] *A Measurement of the t Dependence of the Helicity Structure of Diffractive ρ Meson Electroproduction at HERA*, H1-Coll., C. Adloff *et al.*, DESY 02 – 027, hep-ex/0203022, Phys. Lett. **B539** (2002), 25 - 39.

[7] *Inelastic Photoproduction of J/Ψ Mesons at HERA*, H1-Coll., C. Adloff *et al.*, DESY 02 – 059, hep-ex/0205064, Eur. Phys. J. **C25** (2002), 25 - 39.

[8] *Inelastic Leptoproduction of J/Ψ Mesons at HERA*, H1-Coll., C. Adloff *et al.*, DESY 02 – 060, hep-ex/0205065, Eur. Phys. J. **C25** (2002), 41 - 53.

[9] *Search for QCD Instanton-Induced Processes in Deep-Inelastic Scattering at HERA*, H1-Coll., C. Adloff *et al.*, DESY 02 – 062, hep-ex/0205078, Eur. Phys. J. **C25** (2002), 495 - 509.

[10] *Diffractive Photoproduction of $\Psi(2S)$ Mesons at HERA*, H1-Coll., C. Adloff *et al.*, DESY 02 – 075, hep-ex/0205107, Phys. Lett. **B541** (2002), 251 - 264.

[11] *Measurement of Inclusive Jet Cross Sections in Deep-Inelastic ep Scattering at HERA*, H1-Coll., C. Adloff *et al.*, DESY 02 – 079, hep-ex/0206029, Phys. Lett. **B542** (2002), 193 - 206.

[12] *Search for Odderon-induced Contributions to Exclusive π^0 Photoproduction at HERA*, H1-Coll., C. Adloff *et al.*, DESY 02 – 087, hep-ex/0206073, Phys. Lett. **B544** (2002), 35 - 43.

[13] *Search for Excited Electrons at HERA*, H1-Coll., C. Adloff *et al.*, DESY 02 – 096, hep-ex/0207038, Phys. Lett. **B548** (2002), 35 - 44.

[14] *Isolated Electrons and Muons in Events with Missing Transverse Momentum at HERA*, H1-Coll., V. Andreev *et al.*, DESY 02 – 224, hep-ex/0301030, submitted to Phys. Lett. **B** (2003).

[15] *Measurement of Inclusive Jet Cross Sections in Photoproduction at HERA*, H1-Coll., C. Adloff *et al.*, DESY 02 – 225, hep-ex/0302034, submitted to Eur. Phys. J. **C** (2003).

[16] *Measurement and QCD Analysis of Neutral and Charged Current Cross Sections at HERA*, H1-Coll., C. Adloff *et al.*, DESY 03 – 038, hep-ex/0304003, submitted to Eur. Phys. J. **C** (2003).

[17] Contr. Papers of the H1-Coll., C. Adloff *et al.*, to the Int. Conf. on High Energy Physics, Amsterdam (July 2002).

[18] *Measurement of the Deep Inelastic Scattering Cross Section at $Q^2 \approx 1$ GeV^2 with the H1 Experiment*, (#975 [17]).

[19] *Measurement of the Proton Structure Function Using Radiative Events at HERA*, (#976 [17]).

[20] *Measurement and QCD Analysis of Inclusive Deep-Inelastic Scattering at High Q^2 and Large x*, (#978 [17]).

[21] *Forward π^0 Meson Production at HERA*, (#1000 [17]).

[22] *Forward Jet Production at HERA*, (#1001 [17]).

[23] *Prompt Photon Production at HERA*, (#1007 [17]).

[24] *Measurement of Dijet Cross Sections at low Q^2 at HERA*, (#1009 [17]).

[25] *Measurement of Single Inclusive High E_T Jet Cross Sections in Photoproduction at HERA*, (#1010 [17]).

[26] *Beauty Production in Deep Inelastic Scattering*, (#1013 [17]).

[27] *Inclusive D-meson Production in Deep Inelastic Scattering at HERA*, (#1015 [17]).

[28] *Measurement of D^* - Muon Correlations in Deep Inelastic Scattering*, (#1016 [17]).

[29] *Measurement and NLO DGLAP QCD Analysis of Inclusive Diffractive Deep Inelastic Scattering*, (#980 [17]).

[30] *Measurement of the Diffractive Structure Function at Low Q^2*, (#981 [17]).

[31] *Measurement of Semi-inclusive Diffractive Deep Inelastic Scattering with a Leading Proton*, (#984 [17]).

[32] *Diffractive Dissociation in Photoproduction at HERA*, (#985 [17]).

[33] *Diffractive Photoproduction of Jets at HERA*, (#987 [17]).

[34] *Measurement of Dijet Cross-Sections with Leading Neutrons in ep interactions at HERA*, (#988 [17]).

[35] *Elastic Electroproduction of ρ Mesons at High Q^2*, (#989 [17]).

[36] *Photoproduction of ρ Mesons with a Leading Proton*, (#991 [17]).

[37] *Diffractive J/Ψ Photoproduction at Large $|t|$ at HERA*, (#993 [17]).

[38] *Investigation of Pomeron- and Odderon Induced Photoproduction of Mesons Decaying to Pure Multiphoton Final States at HERA*, (#997 [17]).

[39] *The Photoproduction of Protons at HERA*, (#1002 [17]).

[40] *A Search for Contact Interactions at HERA*, (#979 [17]).

[41] *Electron Pair Production in ep Collisions at HERA*, (#1019 [17]).

[42] *Search for Doubly Charged Higgs Production at HERA*, (#1020 [17]).

[43] *Muon Pair Production in ep Collisions at HERA*, (#1021 [17]).

[44] *Search for W Production in the Hadronic Decay Channel at HERA*, (#1023 [17]).

[45] *A Search for Single Top Production at HERA*, (#1024 [17]).

[46] *A Search for Leptoquarks at HERA*, (#1027 [17]).

[47] *A Direct Search for Magnetic Monopoles*, H1-Coll., A. Aktas *et al.*, Contr. to 11^{th} Int. Workshop on Deep Inelastic Scattering (DIS2003), St. Petersburg RU (April 2003).

[48] *Searches for contact interactions at HERA*, S. Schmitt, Proc. 10^{th} Int. Workshop on Deep Inelastic Scattering (DIS2002), Cracow PL (May 2002), Acta Phys. Polon. **B33** (2002), 3923-3928.

[49] *Heavy Quark Physics at HERA*, F. Sefkow, Proc. XXX^{th} SLAC Summer Institute, Stanford CA, USA (July 2002).

[50] *A Measurement of Beauty Production in High-Energy Positron-Proton Scattering*, Jürgen Kroseberg, PhD-thesis, Zürich 2002.

[51] V. Andreev *et. al.*, Report H1-01/03-607; H1-10/02-606.

[52] *The CIP2k first level trigger system at the H1 experiment at HERA*, M. Urban, J. Becker, S. Schmitt, and U. Straumann, IEEE Trans. Nucl. Sci. **50**, 4 (2003), in print.

[53] *The CIP2k first level trigger system at the H1 experiment at HERA*, M. Urban, J. Becker, S. Schmitt, and U. Straumann, Proc. 2002 IEEE Nucl. Sci. Symp./Medical Imaging Conf., Norfolk VI, USA (November 2002).

[54] *A first level Trigger subsystem CIP2k for the H1 experiment at HERA*, J. Becker, H. Cramer, M. Hildebrandt, K. Müller, S. Schmitt, U. Straumann, M. Urban, and N. Werner, Proc. 8^{th} Topical Seminar on Innovative Particle and Radiation Detectors, Siena I (October 2002), Nucl. Instr. Methods **A**, in print.

[55] *Compact Frontend-Electronics and Bidirectional 3.3 Gbps Optical Datalink for Fast Proportional Chamber Readout*, S. Lüders *et al.*, hep-ex 0107064, Nucl.Instr.Meth.**A484** (2002) 515-527.

[56] H1-Coll., C. Adloff *et al.*, Eur. Phys. J. **C13** (2000) 609.

[57] H1-Coll., C. Adloff *et al.*, Eur. Phys. J. **C19** (2001) 269.

[58] H1-Coll., C. Adloff *et al.*, Phys. Lett. **B479** (2000) 358.

[59] H.L. Lai *et al.*, Eur. Phys. J. **C12** (2000) 375.

[60] H1-Coll., C. Adloff *et al.*, Eur. Phys. J. **C11** (1999) 447; erratum ibid. **C14** (1999) 553.

[61] N. Arkani-Hamed, S. Dimopoulos, and G.R. Dvali, Phys.Lett. **B429** (1998) 263; Phys. Rev. **D59** (1999) 086004.

[62] T. Abe, Comp. Phys. Comm. **136** (2001) 126.

[63] A. Belyaev and N. Kidonakis, preprint hep-ph/0102072.

[64] M. Fontannaz, J.P. Guillet, and G. Heinrich, Eur. Phys. J. **C21** (2001) 303.

[65] A. Courau, and P. Kessler, Phys. Rev. **46** (1992), 117.

[66] H1-coll., C. Adloff *et al.*, Phys. Lett. **B517**, 47 (2001).